Next Materials 13 (2026) 103418

Contents lists available at ScienceDirect

Next Materials

journal homepage: www.sciencedirect.com/journal/next-materials

Research article

Development of sustainable automotive friction components via valorization of agro-waste from Ricinus communis/cashew nutshell/SiC hybrid polymer composites

T.P. Sathishkumar [a,*], P. Senthil Kumar [b], L. Rajeshkumar [c,*], G. Rajeshkumar [d], G. Manikandan [b], R. Gopinath [e]

[a] Department of Mechanical Engineering Kongu Engineering College, Erode, Tamil Nadu, India
[b] Department of Automobile Engineering, Kongu Engineering College, Erode, Tamil Nadu, India
[c] CoE – Advanced Materials Synthesis (CoE-AMS) and Department of Mechanical Engineering, Alliance School of Applied Engineering, Alliance University, Bengaluru, India
[d] Department of Mechanical Engineering, PSG Institute of Technology and Applied Research, Coimbatore, Tamil Nadu, India
[e] Department of Civil Engineering, University College of Engineering, Tindivanam, Tamil Nadu, India

ARTICLE INFO

Keywords:
Agro-waste fibers
Sustainable composites
Physical properties
Tribological properties
Optimization

ABSTRACT

Waste management plays a vital role in valorization of low-performance agricultural waste fibers into high-performance composites. This paves way for the minimization of waste build up and enhancing the sustainable ways for developing environmentally friendly products. The agro waste Ricinus communis (RC) fibers were mercerized with 4% NaOH solution, hybridized with cashew nutshell powder (CNSP) and silicon carbide (SiC) and hybrid composites were developed with constant CNSP content (10 wt%) and varying SiC content (2, 4 and 6 wt%) using hot compression moulding process. The physical, chemical, structural, thermal and tribological properties of the hybrid composite systems were experimentally analyzed. The XRD and FTIR analyses confirmed the improved crystallinity and interfacial interactions specifically for 2 and 4 wt% SiC filled composites. The thermal stability of 4 wt% SiC filled composite was relatively better with a lower residual mass and maximum degradation temperature Tribological properties of the hybrid composites were determined using a pin-on-disc apparatus in dry conditions and optimized using RSM based techniques with Taguchi's L27 design of experiments. The RSM and ANOVA results indicated minimal wear and stable friction in 2 and 4 wt% SiC filled composites. Morphological analysis using SEM depicted that the composites with 4 wt.% of SiC exhibited relatively smoother worn surface with minimal surface abnormalities portraying the better interfacial adhesion. Such low density and sustainable composites find their applications as friction components in industrial wear and automotive applications.

1. Introduction

The growing demand for environmentally sustainable and high-performance mechanical, structural, and tribological materials has accelerated research towards natural fiber reinforced polymer composites (NFRCs) as viable alternatives to synthetic fiber composite materials [1]. Natural fibers derived from renewable and agro-waste sources such as bamboo, banana, jute, flax, sisal, coir, agave, neem, pineapple, and other lignocellulose residues offer advantages including low density, biodegradability, cost-effectiveness, and favourable specific mechanical properties [2]. However, their practical application in tribological environments is limited by their intrinsic drawbacks, such as hydrophilicity, interfacial incompatibility with polymer matrices, and sensitivity to operating conditions. Fiber extraction and chemical modification were critical in governing the structural, mechanical, and tribological response of composites [3,4]. Water retting, steam explosion, and mechanical separation methods were commonly employed to isolate the fibers. The alkali and silane treatments have been widely reported to remove hemicellulose, lignin, waxy impurities, and amorphous phases. Such treatments increased cellulose content, crystallinity index, surface roughness, and effective fiber matrix adhesion, leading to improved stress transfer and interfacial debonding [5,6]. Consequently,

* Corresponding authors.
E-mail addresses: tpsathish@kongu.ac.in (T.P. Sathishkumar), rajeshkumar.l@alliance.edu.in (L. Rajeshkumar).

https://doi.org/10.1016/j.nxmate.2026.103418
Received 24 June 2026; Received in revised form 31 August 2026; Accepted 1 September 2026
Available online 8 September 2026
2949-8228/© 2026 The Authors. Published by Elsevier Ltd. This is an open access article under the CC BY-NC license (http://creativecommons.org/licenses/by-nc/4.0/).

extensive efforts have been focused on improving fiber surface characteristics, interfacial bonding, and composite architecture to achieve reliable physical, mechanical, and wear performance by various fibers and fillers [7,8]. *Ricinus communis* (castor plant) is one of the most economically important non-edible oilseed crops. While the seeds are the primary commercial product, several other parts are utilized, and a significant fraction of the plant becomes agricultural or industrial waste. This makes it a potential candidate for biomass valorization and sustainable composite applications [9]

The tribological behaviors of the polymer composites revealed that the wear rate (W*R*), specific wear rate (SWR), and coefficient of friction (COF) were strongly dependent on applied load, sliding velocity, sliding distance, fiber content, and fiber orientation. The cylinder pin on counter surface showed higher CoF than the ball on counter surface. Increasing load and sliding velocity were produced the frictional heat on the materials surface, resulting in matrix softening, increased debris generation, and transition from mild to severe wear regimes [10,11]. Thus, the reinforcement of different natural fibers, natural and synthetic fibers, or fibers with particulate fillers have gained attention and these approaches aim to balance structural, mechanical, thermal stability and improved tribological performance [12,13]. Studies on hybrid natural fiber materials demonstrated reduced wear loss and improved friction stability compared to single-fiber composites, attributed to synergistic stress redistribution and enhanced load sharing [14].

Sustainable bio particulate reinforcements, such as cashew nutshell (CNS), biochar, coco shell, palm shell, hazelnut bio-based fillers have emerged as promising due to their friction modifying behavior and thermal stability, availability with low cost [15,16]. CNS filler has been widely used to make the brake friction materials with epoxy, thermoplastics, rubber matrices, and bio-resins. CNS-based fillers have enhanced friction stability, reduced wear loss, and improve hardness and thermal resistance through the formation of lubricious carbon-rich tribo-films and improved interfacial adhesion [17–19]. Optimal CNS filler content was typically reported in the range 5–30 wt%, where uniform dispersion and effective stress transfer were achieved. Beyond this range, the filler agglomeration and increased porosity were formed then showed instability thermo mechanical behaviors and affected the tribological performance [20,21]. Alkali-treated CNS fillers further enhanced wear resistance by improving filler-matrix bonding and reducing moisture sensitivity [22].

Many studies on other fillers such as alumina (Al_2O_3), silicon carbide (SiC), Aluminium nitrate are also extensively used to enhance hardness, abrasion resistance, and load-bearing capacity in polymer composites. Both micro- and nano-SiC fillers contribute to improved tribological behavior by restricting matrix deformation, arresting crack propagation, and promoting the formation of protective tribo-films at the sliding interface [23,24]. Numerous studies report optimal SiC content in the range of 4–10 wt%, where tensile strength, hardness, and wear resistance are maximized. Excessive SiC addition beyond this threshold often leads to particle agglomeration, stress concentration, and deterioration of mechanical and wear properties [24,25]. Wear mechanism analyses revealed a transition from severe matrix wear in unfilled composites to mild abrasive and adhesive wear in SiC reinforced composites [26–28]. These improvements directly influenced the wear resistance by reduced fiber pull-out, matrix cracking, and premature surface degradation under frictional loading [29]. Furthermore, the application of statistical optimization techniques such as Taguchi design, ANOVA, grey relational analysis, and response surface methodology (RSM) has enabled systematic identification of dominant wear controlling parameters, with methodological expectations [30–32].

However, despite isolated studies on CNS-filled or SiC-filled composites, a systematic investigation into their combined effect within treated natural fiber reinforced polymer matrices remain limited [9,33]. Moreover, predominant focus on wear performance, with comparatively fewer studies addresses the wear optimization, parameter sensitivity, and wear mechanism correlation in hybrid biocomposites through bio-fibers and fillers. CNS filler in epoxy composites can contribute to damping, friction regulation, and thermal stability, while SiC enhances load bearing capacity and resistance to abrasive wear. These two filler mechanisms can be a potential need for various applications in dry sliding components, clutch, brake materials, and wear critical structural elements [21,22,24,25]. The present work is to study the interaction effect by incorporating the 4% NaOH treated Ricinus communis fiber, CNS and SiC fillers under dry sliding wear test with varying SiC content, applied load and sliding velocities and evaluate their potential to be used as friction components in low mobility vehicles.

2. Materials and methods

2.1. Materials used

The RC fibers were extracted from the Ricinus communis plant stem through manual retting process. The RC plant stems were cleaned by knife, cut into small pieces of 300 mm length and then manually peeled. RC fibers were chemically treated with 4% NaOH to remove their microconstituents and to enhance their structural integrity with the epoxy matrix. The fibers were soaked in 4% NaOH for 24 h and were sun dried thereafter for 2 days. The dried RC fibers were then kept in hot air oven at 60 °C for 2 h to remove any excess moisture [9]. The RC fiber was cut into 1 mm length. The Cashew Nutshell (CNS) filler of 200 μm and Silicon Carbide (SiC) are used as the fillers for the composites development. The SiC filler powder, LR - 250 gm CAS No.409–21–2 (220 Mesh) bought from Bangalore Fine Chemicals, Bangalore. The laboratory LY556 medium viscous epoxy resin and HY951 hardener were bought from Sri Radha Traders, Coimbatore. Table 1 shows the properties of treated RC fiber, CNS filler and SiC filler.

2.2. Manufacturing of composites

The compression moulding process with steel mould (Figure S1) was used to fabricate the hybrid composites. The mould has the length and width of 120 mm × 120 mm, with thickness of 15 mm as shown in Figure S1. The samples were weighed using digital weighing machine and fillers were mixed with the epoxy resin using mechanical stirrer about 10 min to ensure homogenous distribution. The ratio of resin and hardener was maintained as 10:1. Then, the treated RC fibers were

Table 1
Properties of fiber and fillers.

Properties	RC Fiber [9]	CNS filler [20,21,33]	SiC [23,25,29]
Cellulose (wt%)	78.3	64.57	-
Hemicellulose (wt%)	30.2	0.70	-
Lignin (wt%)	9.8	24.31	-
Density (g/cc)	1.26	0.337	3.25
Diameter (μm)	227.4	-	-
Single fiber Tensile Strength (MPa)	428 – 452	-	-
Single fiber Young's Modulus (GPa)	9.9 – 11.1	-	-
Single fiber Elongation (%)	1.52	-	-
Crystallinity Index (%)	40–42	-	-
Crystallinity Size (nm)	28–30	-	-
Thermal stability (° C)	380	-	-
Shore hardness (HS)	-	38–50	110–120
Particle size (μm)	-	150–200	-
Tensile Strength (MPa)	190–280	-	-
Thermal stability (° C)	-	320	-
Thermal Conductivity (W/m. K@25°C)	-	-	60–120
Thermal stability (° C)	-	-	1500
Poisson's ratio	-	-	0.14
Coefficient of Thermal Expansion (10^{-6}/K)	-	-	2.3–4

placed in the mould, and the fillers-resin mixture was poured in the mould cavity. The closed mould was subjected to 35 MPa pressure and 160 °C for 4–5 h. These process parameters were selected as they result in complete curing of composites, due to higher glass transition of epoxy resin, better flow of resin within the composites and improved mechanical properties [34,35]. Post curing was carried out for 3 h after the withdrawal of application of temperature and pressure. Then the cured composite specimen was used to derive the test specimens for physical and tribological tests. Three set of composites plates were prepared for each composition (as shown in Fig. 1), and three pins were cut from each sample for conducting wear tests. Table 2 shows the compositions of composites.

2.3. Physical properties

2.3.1. Density analysis

The physical density of the composite samples was determined using Archimedes' principle [36,37] with medium of distilled water according to ASTM D792 (Figure S2), and theoretical density was calculated based on the rule of mixtures (Eq. 1).

$$\rho a = \frac{\rho w \, Wa}{Wa - Ww} \quad (1)$$

Where, ρ_a is actual density of composite (g/m^3), ρ_w is the density of distilled water (g/m^3), W_a is weight of the sample in air (g) and Ww is weight of the sample in water (g).

The theoretical density (ρ_t) of the composite material was determined by using the following Eq. 2.

$$\rho t = \frac{1}{[(W + /\rho f) + (Wm/\rho m)]} \quad (2)$$

Where, W_f is the weight fraction for fiber; W_m is the weight fraction for matrix; ρ_f is the density of fiber and ρm is the density of matrix. Volume fraction of voids (V_v) was calculated by using the following Eq. 3.

$$Vv = \frac{\rho t - \rho a}{\rho t} \quad (3)$$

Table 2
Weight proportion of the composites.

Weight proportion (%)					
	Samples Grouped	Fiber weight (%)	CNS Filler weight (%)	SiC Filler weight (%)	Resin weight (%)
Sample 1	S1	50	10	-	40
Sample 2	S2	50	10	2	38
Sample 3	S3	50	10	4	36
Sample 4	S4	50	10	6	34

2.3.2. Water absorption test

The water absorption test was performed to assess the moisture uptake by composites as per ASTM D570. Composite samples (Figure S3) were immersed in water at room temperature, and their weights were recorded at regular time intervals using a three-digit precision weight balance machine [38]. Before weighing, surface moisture is removed by wiping the samples surfaces using tissue paper. The percentage of water absorption was calculated using Eq. 4.

$$\% \ \textit{Water Absorption} = [\frac{(Mw - Md)}{Md}]x100 \quad (4)$$

Where, Mw is the weight of the wet sample and Md is the weight of the dry sample.

2.4. Thermogravimetric analysis (TGA)

TGA was performed using SEIKO TGA/DTA 6200 analyser to determine the thermal stability of the RC fiber and the composite samples. The powdered fiber composite specimens were heated from 30°C to 800°C in a nitrogen atmosphere to prevent oxidation. The heating rate was set to 20 °C/min, and weight loss was recorded as a function of temperature to analyse the decomposition behaviour [32,34,39].

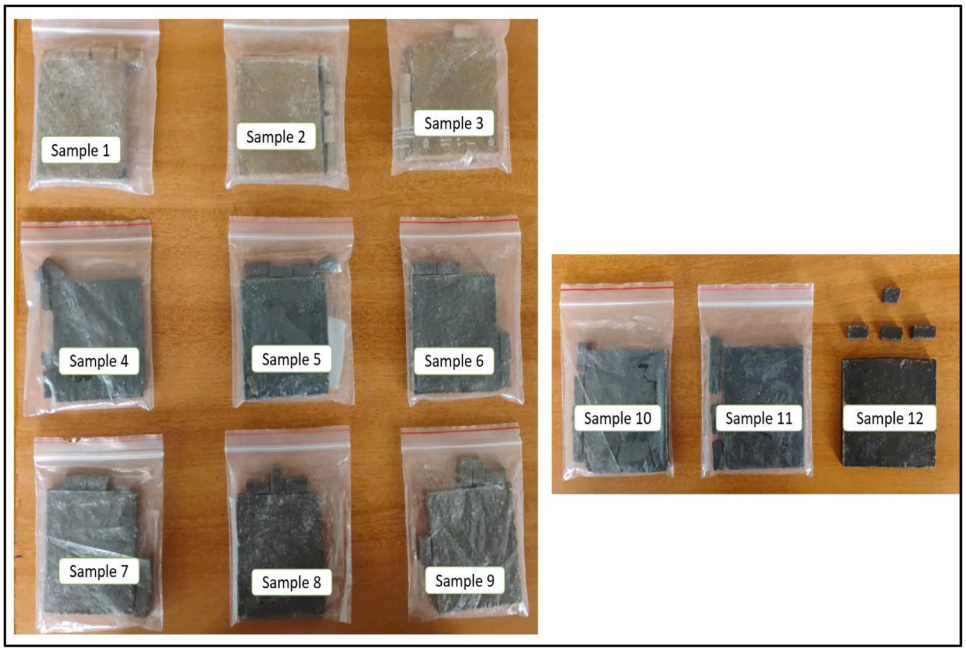


Fig. 1. Samples for wear test.

2.5. Characterization

2.5.1. Fourier-Transform Infrared (FTIR) spectroscopy

The functional groups present in raw, alkali treated fibers and the composite samples were analyzed using FTIR-6300 spectrometer to study their presence of functional modifications due to chemical treatment. About 5–10 mg of each fiber and composite samples was milled, mixed with Potassium Bromide (KBr), and pressed into a disc of the equipment. Spectra were recorded at scanning speeds of 2 mm/sec, covering the wavenumber range of 400–4000 cm^{-1} with a resolution of 4 cm^{-1} [22].

2.5.2. X-ray diffraction (XRD) test

XRD analysis was used for the calculation of the crystallinity index through the position and intensity of diffraction peaks, which indicates the proportion of crystalline material in the fiber and the composite samples. Anton Paar XRDynamic 500 X- ray diffractometer is used for testing the fiber and hybrid composites [22]. Specifications of X-ray source type is Primux 3000, X-ray generator up to 3 kW, voltage of 20–60 kV, and 2–50 mA, Bragg's angle of 5 ° to 80 ° and X-ray wavelength of 1.54 Å.

2.5.3. Scanning electron microscopy (SEM)

The microstructure of fiber and the surface morphology of the composite materials were examined using a SEM coupled with Energy Dispersive X-ray spectroscopy (EDX). SEM images were used to study the fracture mechanisms, fiber matrix interface, and wear tracks on the composite surfaces [24]. EDX was utilized to determine the elemental composition at the composite surface. JCM-7000 Benchtop SEM coupled with EDX equipment having specifications of landing voltage of 15 kV/ 10 kV/ 5 kV, Tungsten filament electron gun and Magnification of x 20, 000 is used for scanning the samples. The elemental composition of RC fiber and their composites were examined using EDX.

2.6. Wear analysis

The dry sliding wear test was conducted in DUCOM pin-on-disc wear testing machine, under room temperature conditions (Figure S3). The testing was performed according to the ASTM G99–17 standard. Test samples were made with dimensions of φ10 × 30 mm length [26]. The sample was fixed in a holder mounted on the testers flexible arm and brought into contact with a hardened steel disc of track diameter 80 mm rotating at varying speeds. A lever mechanism was used to apply normal loads of 10 N, 20 N, and 30 N. The tests were conducted under varied sliding velocities (Table 3), and the weight loss of the specimen was measured after each cycle using an electronic precision balance [36]. Based on this data, wear rate (WR), Specific Wear Rate (SWR), and Coefficient of Friction (COF) were calculated [10,17,18,20]. Table 3 shows the parameters considered for the sliding wear testing of the RCC by systematically varying the load and velocity to identify optimal conditions for minimizing wear. The following Eq. 5 is used to calculate the specific wear rate (SWR) of the RC fiber hybrid composites samples where V_L denotes the wear volume loss, X_D denotes the sliding distance, P denotes the applied load.

$$SWR = \frac{V_L}{X_D \times P} \quad (\mathrm{mm3}/\mathrm{N.m}) \tag{5}$$

Table 3
Parameters for wear testing of the composites.

Load (N)	Speed (rpm)	Sliding Velocity (m/s)	CNSP filler (wt %)	SiC filler (wt %)
10	500	2.1	10	2
20	1000	4.2	10	4
30	1500	6.3	10	6

2.7. DOE and optimization

CCD (Central composites design) based Response Surface Methodology (RSM) [39] is to optimize the influence of several factors such as SiC filler loading, testing speed and testing load (Applied load) on tribological behaviour of the composites (Fig. 2).

A standard structure CCD for the factors typically requires fewer runs that include centre point replicates is adopted. A 27 experimental (L27) run design is used for model and involve a full factorial design with a high number of center point replicates and categorical factors [39,40]. The 27 experiments run involves the three independent factors (variables). For statistical modelling, each process parameters were coded at three levels of "–1, 0, and + 1", representing the low, central, and high levels, respectively (Table 4). The parameters and the coded values used in the RSM design for the RC composites for the wear tests are given in the Table 6. The general form of the full quadratic model for n factors is represented in the Eq. 6 [40]:

$$Y = a_0 + \sum_{i=1}^{k}(b_i X_i) + \sum_{i,j}^{k}(b_{ij} X_i X_j) + \sum_{i=1}^{k}(b_{ii} X_i^2) \tag{6}$$

Where, Y denotes the predicted response, $X_ı$ and X_j are the independent coded variables (i and j ranging from 1 to k), a_o is the intercept, b_i represents the linear coefficients, b_{ij} indicates interaction coefficients, and b_{ii} corresponds to quadratic coefficients.

2.8. Analysis of variance (ANOVA)

The ANOVA provides the statistical details including degrees of freedom (DF), sum of squares (SC), mean squares (MS), F-values (F), and probability (P), along with the contribution percentage of each factor toward the total variation. The significance of each model term was evaluated using p-values and F-values. A p-value less than or equal to 0.05 indicates that the factor significantly influences the response at a 95% confidence level. Similarly, higher ratio of variances (F-values) denotes greater significance of the corresponding variable in the model [41,42]. Model adequacy and accuracy were assessed using statistical coefficients such as the correlation coefficient (R), coefficient of determination (R^2), adjusted R^2 ($R^2_{ad_j}$), and predicted R^2 (R^2_{pred}). The R value measures the strength and direction of a linear relationship between the variables. The R^2 value represents the proportion of total variation explained by the model, and values approaching unity indicate a strong correlation between experimental and predicted results, reflecting good model fit [42]. The adjusted R^2 improves the number of predictors, while the predicted R^2 evaluates the model's predictive capability.

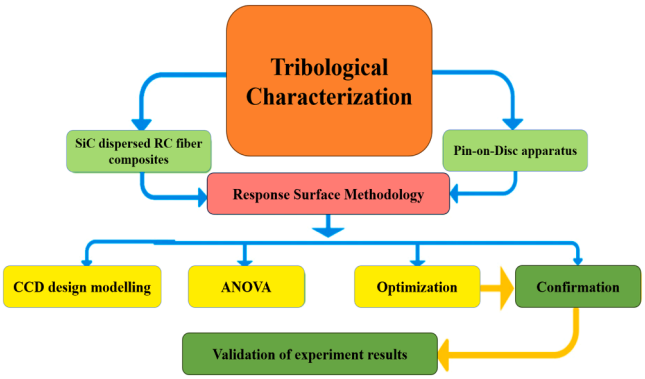


Fig. 2. Optimization methodology.

Table 4
Parameters and the coded values used in the RSM design for wear test.

Name (Code)	Parameter	Units	Low (-1)	Medium (0)	High (+1)	- α	+ α
A	Load	N	10	20	30	0	40
B	Velocity	m/s	2.1	4.2	6.3	0	8.4
C	SiC filler	%	2	4	6	0	8

Table 5
Density analysis of SiC/CNSP-based hybrid RC composites.

Sample	Measured Density (g/cm^3)	Theoretical Density (g/cm^3)	Void (%)
1	1.582	1.596	0.87
2	1.601	1.617	0.99
3	1.622	1.641	1.15
4	1.640	1.664	1.44

Table 6
Water absorption of SiC/CNSP-based hybrid RC composites.

Sample	Water absorption (%)
1	1.66
2	2.05
3	2.36
4	3.38

3. Results and discussion

3.1. Characterization of hybrid RC composites

3.1.1. Microstructural analysis of RCC

The microstructure of Sample 1 reveals the presence of noticeable pores and cavities (Fig. 3a-d). These voids are likely the result of air entrapment or incomplete resin infiltration during the manufacturing process [32,34,37]. The presence of single filler provides less bonding between reinforcement and matrix which may compromise the wear and friction properties of the composite. The EDX spectrum confirms the presence of various elements in the RCC without SiC. The CNSP and RC fiber are natural sources which confirm by presence of carbon and oxygen. These are the major contribution in the composites as shown in EDX graph (Fig. 3e).

Fig. 4 shows the microstructure sample 3 and sample 4 with 4 wt% and 6 wt% of SiC fillers respectively and its corresponding EDX spectrum portraying the presents of various elements. It shows the homogenous distribution of SiC particles throughout the epoxy matrix with CNSP filler. As the SiC content increases few interfacial pores are observed around the periphery of the SiC particles. At higher filler concentrations (6 wt% SiC), slight clustering or agglomeration of SiC particles is observed, which can lead to localized stress concentrations and potential deterioration of tribological performance [25]. Despite the formation of pores, the matrix shows good wetting behaviour with SiC particles at moderate filler levels, suggesting an acceptable level of interfacial bonding [43]. Hence, a uniform dispersion of SiC particles can be achieved at sample 3 with 4 wt% SiC particles.

3.1.2. XRD analysis of hybrid composites

The XRD spectrum of RCC with CNSP and varying SiC filler contents are shown in the Fig. 5. As the SiC content increases from 2 wt% to 6 wt %, additional peaks associated with silicon carbide become evident in the diffraction pattern [22,27]. The percentage of crystallinity and crystallinity size are around 20.07% and 26.42%. A notable observation is the reduction in the intensity of the initial diffraction peak around 20°. This decrease in peak intensity with increasing filler content is attributed due to the extensive surface coverage by the dispersed SiC particles, which reduces the exposure and detectability of RC fiber peaks in the XRD spectrum.

Fig. 5 shows the diffraction intensity versus 2θ for three different hybrid RC composite samples. Peak position of the composites occurs around $2\theta = 20^\circ$ and the most prominent diffraction peak have seen across all samples. Sample 2 shows the highest intensity (nearly 200 counts), indicating higher crystallinity or better-ordered structure compared to the others. As the SiC content increases in the composites, the peaks generally show decreasing intensity. This trend suggests SiC dispersion suppresses RC fiber peak exposure, reducing crystallinity or making fiber-related peaks less visible due to particle coverage. Broad Peaks at higher 2θ (30°– 80°) show slight rise in intensity in this region, particularly in 4 wt% SiC and 6 wt% SiC. These may correspond to amorphous or less ordered regions, or minor contributions from SiC particles dispersed in the matrix [44].

3.1.3. FTIR Analysis of hybrid composites

FTIR spectra analysis shows the effect of CNSP and varying SiC filler loading on the chemical structure of RCC. Peaks in the FTIR spectra represent specific functional groups, and variations in peak intensity [22,26] and position indicate chemical changes or interactions due to filler addition (Fig. 6). Sample 2 exhibit slight intensity increase in the O–H region (3330 cm^{-1}), indicating potential hydrogen bonding due to filler interaction. C═O peak (1735 cm^{-1}) becomes more pronounced, suggesting enhanced matrix filler interaction or improved exposure of hemicellulose groups. New peak or shoulder near 1100–1150 cm^{-1} might be due to Si–O stretching from SiC or interaction with fiber matrix. This indicates that at 2 wt% SiC, the filler begins to interact chemically and possibly improving interfacial bonding. In sample 3, the O–H and C═O peaks are more intense, suggesting enhanced matrix modification and slight shift in the aromatic region (around 1600 cm^{-1}), indicating possible lignin and filler interaction. The Si–O stretch (around 1100–1150 cm^{-1}) is clearer, confirming the presence of SiC and its chemical involvement. In sample 3, the significant bonding occurs, suggesting optimal interaction between filler and matrix, the chemical compatibility is maximized. Sample 4 shows peak intensities in the O–H and C═O regions start to decline and broaden, suggesting possible agglomeration or saturation effect of the filler. Si–O region shows a stronger signal, confirming increased SiC content. However, peak broadening and decreased sharpness indicate disruption in uniform interaction or potential phase separation. In sample 4, the interaction may become less effective due to filler saturation, and agglomeration, slightly hindering efficient matrix bonding.

3.2. Physical properties of hybrid RC composites

3.2.1. Density of the composites

The results of the measured density, theoretical density, and percentage void content of RCC with varying SiC filler and CNSP contents are represented in Table 5. The measured density of the composites shows a gradual rise with the incorporation of SiC fillers, which is attributed to the higher density of SiC compared to epoxy and RC fibers. The measured density (1.58–1.64 g/cm^3) and the theoretical density (1.59–1.66 g/cm^3) of the composites for the various SiC wt% are provided the use of composites for lightweight applications that influences mechanical performance, weight-to-strength ratio, and overall structural behaviour [36,37]. Density steadily increased with increasing SiC content. Due to the higher intrinsic density of the filler, an increase in void content is also noted. The increase in void content might reduce the strength by weakening interfacial adhesion due to pore formation, air entrapment or incomplete resin infiltration. However, the void percentage was found to be under 2% in all the cases denoting the better interfacial adhesion between the composite constituents.

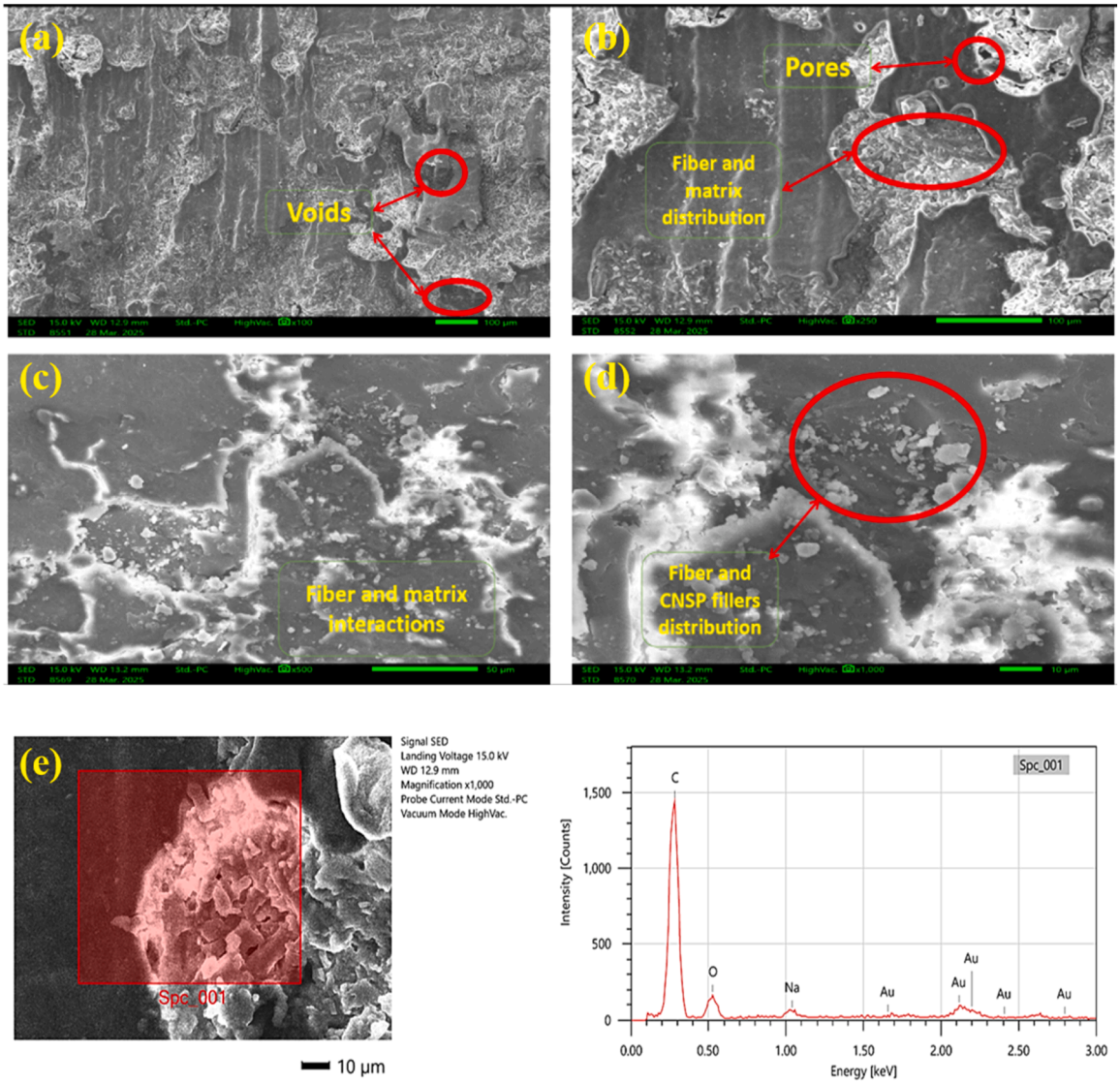


Fig. 3. SEM and EDX spectra of RCC without SiC filler (a-d) Morphology of the composites, (e) EDX spectrum of the composites.

3.2.2. *Water absorption behaviour of the hybrid RC composites*

The SiC dispersed RC composites were tested for water absorption behaviour and their corresponding values are shown in Table 6. Although the chemical treatment improves the interfacial bonding, the presence of micro gaps, pores and voids provide pathways for water molecules to penetrate, thereby increasing the water absorption [22]. Moisture causes the matrix to swell, softens, and eventually develop cracks resulting in poor structural integrity of the composite [25,36]. At lower filler loadings (0 and 2 wt%), with the resin distributions and the fiber interactions, the water uptake is lesser although irrespective presence of micro cracks, pores and voids in the composites. However, at higher filler loadings (4 and 6 wt%), the increase in voids dominates over the benefits of better bonding, leading to higher water uptake.

3.3. *Thermal analysis of hybrid RC composites*

TGA/DTG analysis (Fig. 7) shows the thermal degradation of CNS and varying SiC fillers dispersed RCC. It could be noted from Table 7 that sample 1 has the onset degradation at 339 °C peak degradation (DTG inflection) at 373.7 °C, end of degradation at 405 °C with the mass loss of 54.19% and 38.00% in main stage. The residual mass at 799.5 °C is 43.69% showing a limited thermal resistance due to absence of SiC particles. RCC with 2 wt% SiC has the onset degradation at 355.7 °C, peak degradation at 388 °C, end of degradation at 428 °C with mass loss of 79.36% total, 68.61% in main stage and residual mass 13.40%. Slight improvement in thermal stability occurred due to addition of SiC. However, the significant increase in mass loss suggests volatile degradation products are more prevalent, and the lower residual mass indicates less char or filler remaining [6,8]. Thermal stability of the composites was evaluated from both the resistance to the initiation of thermal degradation and the stability of the residual fraction at elevated temperatures. The 4 wt% SiC composites exhibited the highest onset degradation temperature (358.4 °C) and peak degradation temperature (388.5 °C), compared with 339.0 and 373.7 °C for the unfilled composite, indicating that the incorporation of 4 wt% SiC effectively delayed the initiation and maximum rate of degradation. This behaviour can be attributed to the barrier effect of well-dispersed SiC particles, which restricts polymer-chain mobility and heat/mass transfer, together with improved interfacial interactions within the composite.

However, the 4 wt% SiC composites exhibited a higher total mass loss (89.92%) and lower residual mass (4.99%) than the other compositions. Thus, its superior performance should be interpreted specifically in terms of resistance to the onset of decomposition rather than residue stability at the end of the TGA cycle. The lower residual mass suggests that the organic constituents underwent complete decomposition at higher temperatures. Therefore, the 4 wt% SiC composition

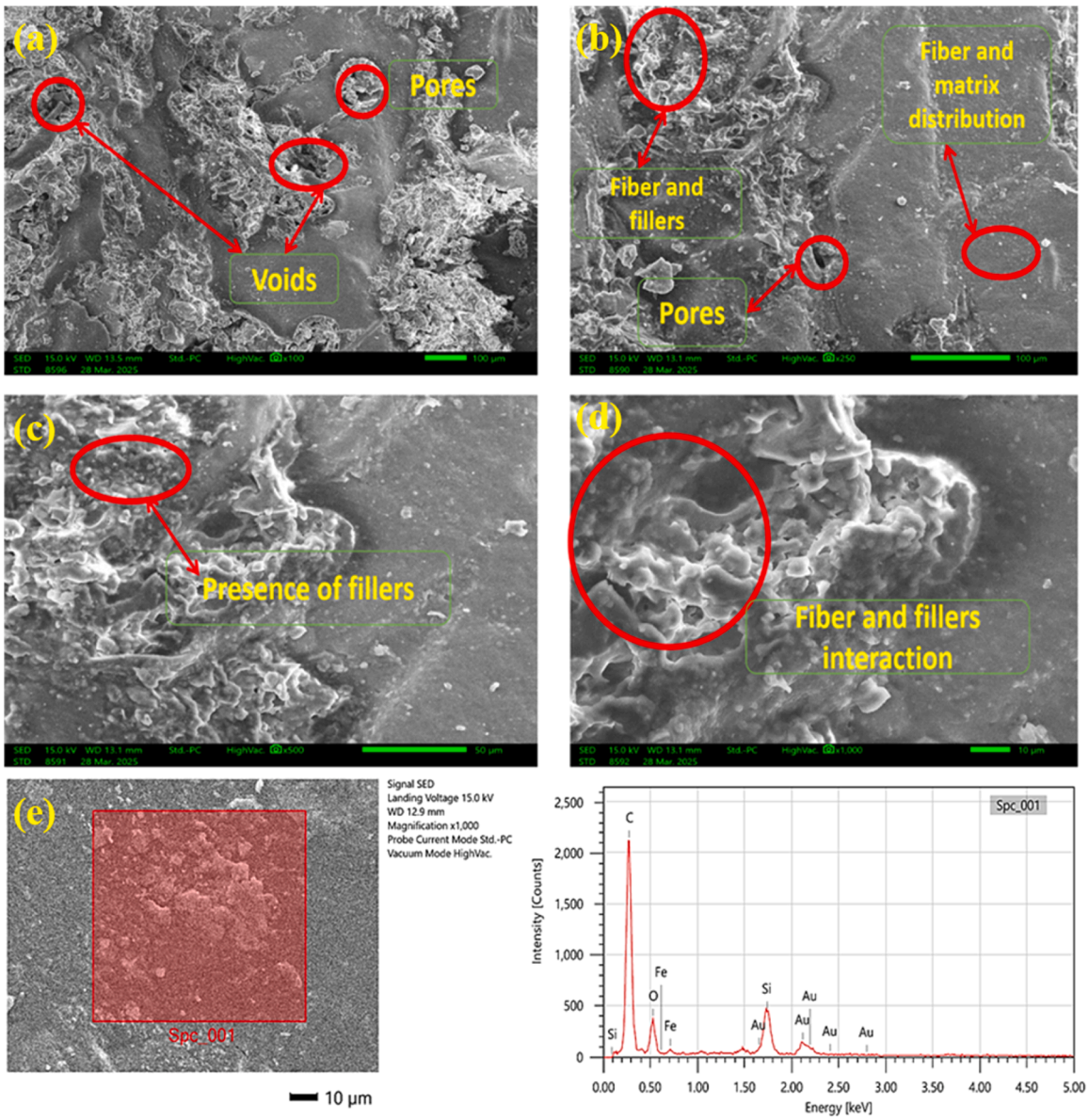


Fig. 4. SEM and EDX spectra of SiC/CNSP-based hybrid RC composites (a, c) 4 wt% SiC composites, (b, d) 6 wt% SiC composites, (e) EDX spectra of 4 wt% SiC composites.

demonstrates enhanced resistance to initial thermal degradation, while the residual fraction indicates comparatively lower stability of the decomposition products at prolonged high-temperature exposure. This distinction provides a more comprehensive interpretation of the thermal behaviour of the SiC-reinforced hybrid composites. RCC with 6 wt% SiC gives the onset degradation at 354.6 °C, inflection point at 385.7 °C, mass loss of 83.33% and residual mass 9.41%. The degradation was later due to the presence of fiber and the fillers, also residues are little higher than the RCC with 4 wt% SiC. Thermal stability slightly improves with the addition of SiC, especially between 0% and 2 wt% (Table 7). The 2 wt% and 4 wt% have optimized thermal stability with high end degradation above 425 °C. However, higher SiC content of 6 wt% leads to greater mass loss and lower residual mass, suggesting more complete degradation of the organic matrix. The DTG curve shows more defined and sharper peaks, indicating a faster degradation rate and also increased SiC does not significantly shift thermal stability but reduces the residual inorganic fraction [7,24].

3.4. Wear parameters of RCC

The major observations are found that the increasing filler contents are gradually increasing, the wear behaviour of composites, at higher loads and speeds [28,41]. Effect of varying loads shows that the wear rate increases significantly with load at a constant speed and filler content (Table 8). The 2 wt% SiC filled RCC at 2.1 m/s shows the *WR* at varying loads of 10 N (279.96 mm^3), 20 N (317.61 mm^3/m), 30 N (360.60 mm^3/m). The SWR value remains relatively stable with increasing load at constant speed but increases slightly. At higher loads the FF and COF both increased with load, due to higher contact forces.

Effect of SiC filler content shows that, the *WR* rises from 279.96 mm^3 /m (2 wt% SiC) to 283.24 mm^3 /m (6 wt% SiC) for 10 N and 2.1 m/s, while the lower *WR* of 194.65 mm^3 /m (4 wt% SiC) is observed. SWR rises from 0.0193 to 0.0491 mm^3 /Nm for 2–6 wt% SiC filler content. Although, the FF increases from 2.98 N to 10.93 N, and COF remains relatively stable between 0.2842–0.3588. Thus, higher SiC improves hardness and frictional stability but increases abrasive interactions, influencing wear mechanisms [25]. Effect of sliding velocity

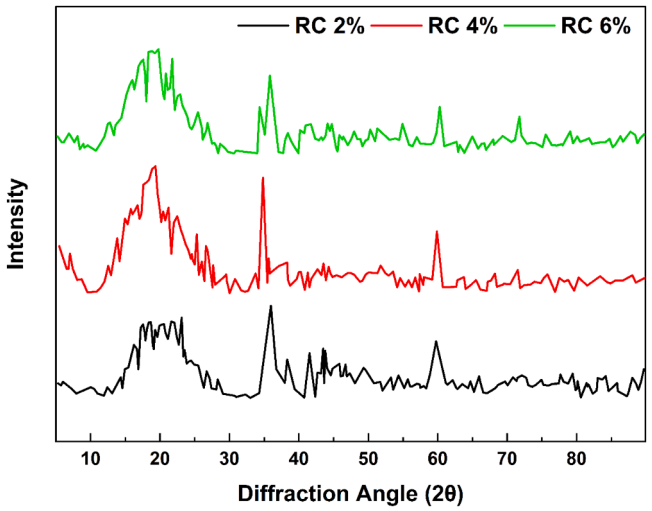


Fig. 5. XRD peaks of SiC/CNSP-based hybrid RC composites.

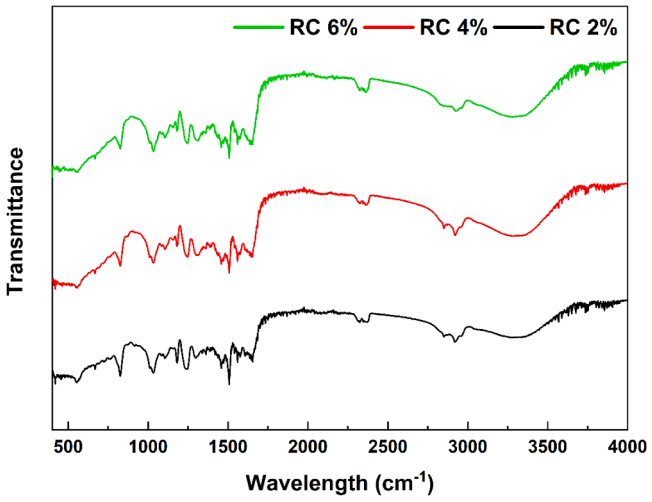


Fig. 6. FTIR analysis of SiC/CNSP-based hybrid RC composites.

at varying velocities shows WR increases with speed, particularly at high loads. It is found that the 2 wt% SiC and 30 N shows varying velocities 360.6 mm^3 /m (2.1 m/s), 338.6 mm^3 /m (4.2 m/s) and 361.2 mm^3 /m (6.3 m/s). SWR increases significantly at higher velocities, particularly for 6 wt% SiC, suggesting more thermal degradation and surface fatigue at higher speeds, and COF decreases at higher speeds for 2 wt% SiC but in general increases at higher filler content and velocity [23,27]. Fig. 8 (a-c) shows that the WR, SWR, and COF results are lower at low filler content (2 wt% and 4 wt%), lower loads, and moderate speeds with reduced wear and friction. At 6 wt% SiC, 30 N, and 6.3 m/s the highest WR of 389.97 mm^3 , highest SWR of 0.0491 mm^3 /Nm and highest COF of 0.3588 are noted. Thus, high filler content, load, and velocity together influence the wear performance, with increased surface heating and fiber matrix debonding [25].

3.5. Statistical analysis of RCC

The WR is primarily influenced by load (A), showing strong statistical significance with F-value of 89.39 and a p-value < 0.0001 (Table 3.5) indicates as the most dominant factor in controlling the wear intensifying the abrasive interaction between the composite surface and the counter-face, at higher loads [42]. Sliding velocity (B) also plays a significant role ($p = 0.004$), indicating that increased velocity elevates the thermal and mechanical stresses at the interface, contributing to higher wear. The linear effect of SiC filler (C) is not significant ($p = 0.4329$), but the quadratic contribution of SiC (C^2) is highly influenced ($p < 0.0001$). This highlights a non-linear behaviour where wear resistance is optimized at a certain SiC concentration. For SWR, both load (A) and SiC filler (C) exhibit strong significance (Table 9). Load contributes with F-value of 105.09 ($p < 0.0001$), along the most dominant contribution from the linear effect of SiC filler $F = 319.39$ ($p < 0.0001$), confirming that increasing SiC content substantially enhances wear resistance. Sliding velocity is also significant ($p = 0.002$), demonstrating that SWR is sensitive to velocity induced temperature rise and material softening. The FF is highly dominated by the load (A), a higher F-value of 3950.76 ($p < 0.0001$) is reflecting the direct proportionality between normal load and frictional resistance (Table 9). SiC filler (C) is also significantly affect the FF ($p = 0.0002$), suggesting that the presence of hard SiC particles reduce the adhesion and stabilizes friction. At 2 wt% SiC, the reinforcement is sufficient to improve the wear resistance compared to the unfilled composite but the availability of SiC filler is meagre, limiting the formation of an effective load-carrying network. Meanwhile in 4 wt% SiC composite a more uniform dispersion of SiC particles and stronger fiber–matrix interfacial bonding was observed, resulting in increased resistance to matrix deformation, reduced ploughing, and enhanced protection against material removal during sliding. These microstructural characteristics contribute to the superior tribological performance observed at 4 wt% SiC as witnessed in Fig. 13. Beyond this concentration (6 wt%), particle agglomeration and increased stress concentration are likely to deteriorate the interfacial integrity, thereby reducing the wear resistance. The COF is significantly influenced by load (A), SiC filler (C), and the BC and B^2 terms. Load exhibits high significance $F = 50.66$ ($p < 0.0001$), showing that COF increases due to enhanced interfacial contact (Table 9). SiC reinforcement exerts an even stronger effect with $F = 139.15$ ($p < 0.0001$), demonstrating its ability to reduce COF by lowering adhesive friction through surface hardening. The regression equations of the wear parameters for the RCC were also obtained.

The regression equations (Eqs. 7, 8, 9) with quadratic functions of RC composites for the wear parameters are expressed below:

$$\text{Wear Rate (WR)} = +236.38 + 31.31\,A + 11.01\,B + 2.66\,C + 4.49\,AB - 3.00\,AC + 10.04\,BC - 3.78\,A^2 + 22.63\,B^2 + 71.98\,C^2 \quad (7)$$

$$\textit{Specific Wear Rate (SWR)} = +0.0335 + 0.0048\,A + 0.0017\,B + 0.0083\,C + 0.0009\,AB + 0.0016\,AC - 0.0010\,BC - 0.0010\,A^2 + 0.0018\,B^2 - 0.0006\,C^2 \quad (8)$$

$$\textit{Coefficient of Friction (COF)} = +0.3386 + 0.0078\,A - 0.0018\,B + 0.0130\,C + 0.0003\,AB - 0.0029\,AC + 0.0140\,BC + 0.0044\,A^2 - 0.0137\,B^2 - 0.0047\,C^2 \quad (9)$$

3.6. Optimization model validation

To verify the reliability of the developed regression model, additional confirmation experiments were performed using a new set of parameter combinations that differed from those employed during model development [39]. The selected parameter levels for the validation trials are summarized (Table 10), and the corresponding experimental responses were compared with the model-predicted values [40,44]. Although the maximum prediction error for wear rate (WR) was found to be 8.78%, this value is considered acceptable for tribological experiments, where wear measurements due to the higher experimental variability and dependence of various factors. Moreover, the observed error corresponds to relatively high wear rate values such that a small variation in wear values results in a larger error percentage. However, it could be seen from the table that the prediction errors for the specific wear rate (2.12%) and coefficient of friction (2.50%) are considerably

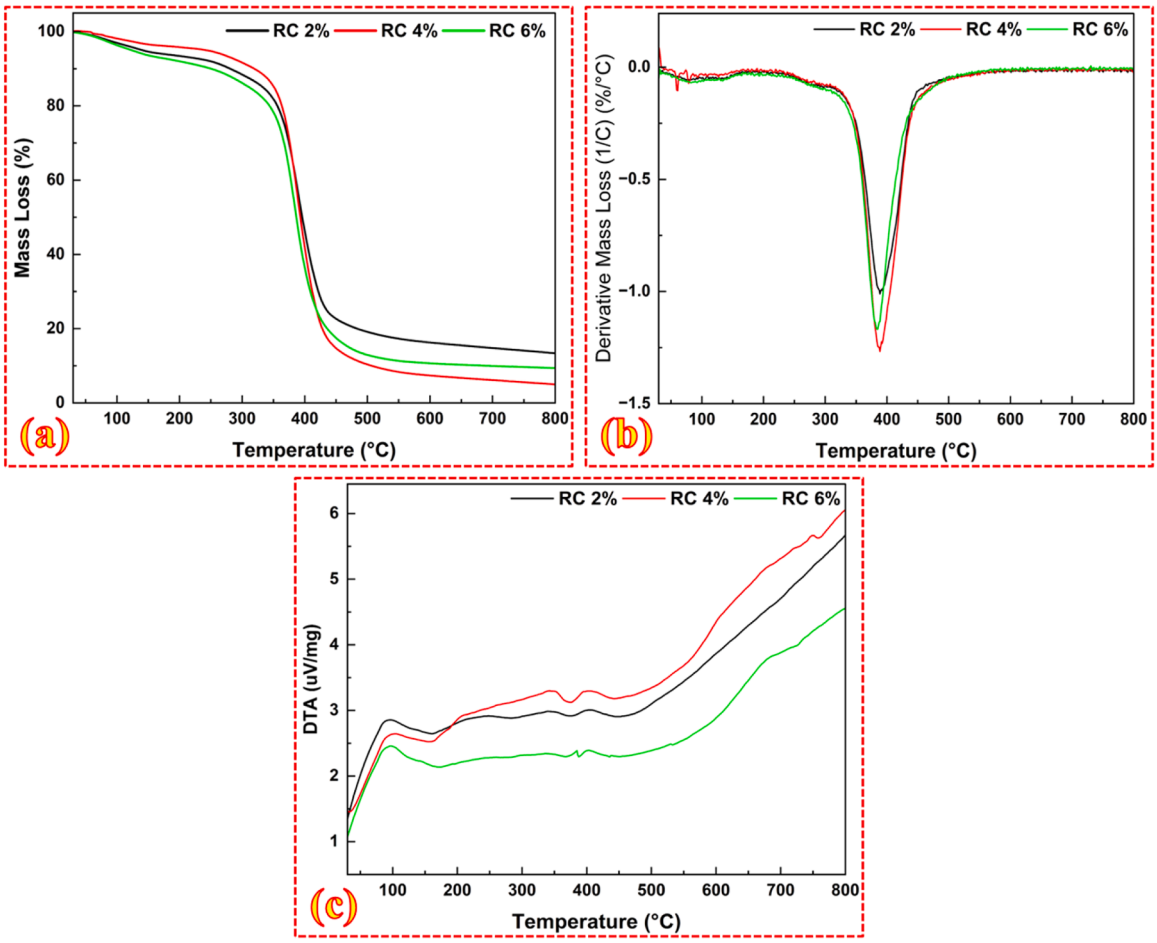


Fig. 7. Thermal properties of SiC-CNSP based hybrid RC composites (a) TGA curve, (b) DTG curves, (c) DTA curves.

Table 7
Thermogravimetric analysis of RCC.

SiC (wt%)	Onset (°C)	Peak (°C)	End (°C)	Mass Loss (%)	Residual Mass (%)
0	339.0	373.7	405.0	54.19	43.69
2	355.7	388.0	428.0	79.36	13.40
4	358.4	388.5	426.1	89.92	4.99
6	354.6	387.7	419.6	83.33	9.41

lower, demonstrating the predictive capability of the developed model. These deviations fall within an acceptable range and the predicted values, confirming the RSM based ANOVA modelling approach is accurate and reliable for estimating wear rate and frictional responses of SiC dispersed RCC.

3.7. 3D response surface analysis

The parity plots of W*R*, SWR, FF and COF compared predicted and actual experimental wear values, showing data points aligned closely along the diagonal reference line (Figs. 9–11). This strong correlation verifies the reliability of the developed model, as most points clustered near the regression line [32,40]. This indicates high model robustness and reliability in capturing the wear behaviour. The close clustering of around the line suggests that the predictive model reliably captures the wear behaviour across low to high W*R* values.

The 3D response surface analyses of wear rate (W*R*), specific wear rate (SWR), frictional force (FF), and coefficient of friction (COF) showed that the significant influence of SiC filler content and operating

Table 8
Wear analysis of RCC-CNS-Si hybrid composites.

Sl. No.	Load (N)	Velocity (m/s)	Filler (%)	WR (μm)	SWR (mm^3/Nm)	COF
1	10	2.1	2	279.9555	0.0212	0.3184
2	20	2.1	2	317.6104	0.0226	0.3222
3	30	2.1	2	360.6034	0.0260	0.3366
4	10	4.2	2	284.5541	0.0193	0.3112
5	20	4.2	2	316.1136	0.0241	0.3175
6	30	4.2	2	338.5874	0.0271	0.3375
7	10	6.3	2	279.0436	0.0258	0.2842
8	20	6.3	2	326.7319	0.0290	0.3006
9	30	6.3	2	361.2009	0.0312	0.3042
10	10	2.1	4	218.9599	0.0286	0.3215
11	20	2.1	4	266.1461	0.0352	0.3286
12	30	2.1	4	280.9399	0.0324	0.3414
13	10	4.2	4	194.6573	0.0276	0.3380
14	20	4.2	4	219.1654	0.0359	0.3419
15	30	4.2	4	234.6475	0.0401	0.3528
16	10	6.3	4	239.7717	0.0281	0.3209
17	20	6.3	4	282.6219	0.0363	0.3134
18	30	6.3	4	303.6366	0.0421	0.3334
19	10	2.1	6	291.423	0.0359	0.3240
20	20	2.1	6	302.3537	0.0422	0.3147
21	30	2.1	6	323.2651	0.0488	0.3311
22	10	4.2	6	283.2465	0.0342	0.3454
23	20	4.2	6	315.6588	0.0381	0.3498
24	30	4.2	6	349.9889	0.0458	0.3514
25	10	6.3	6	307.6924	0.0362	0.3426
26	20	6.3	6	348.6805	0.0455	0.3482
27	30	6.3	6	389.9724	0.0491	0.3588

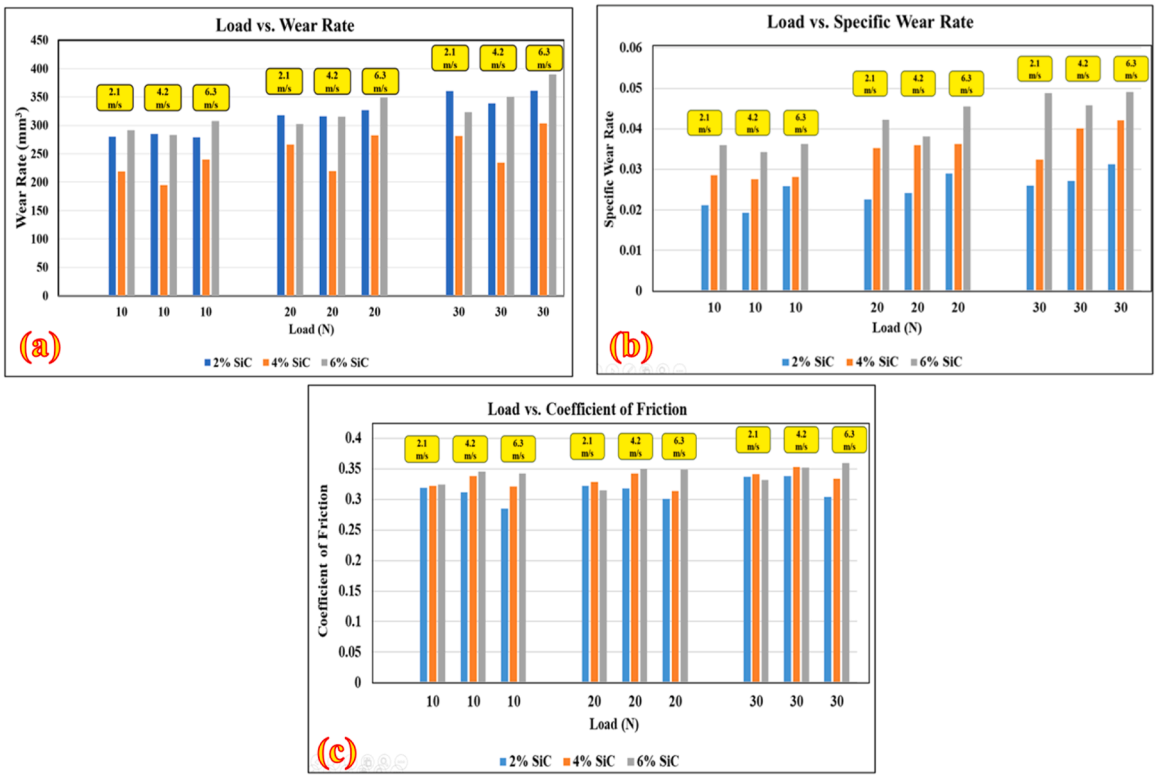


Fig. 8. Wear behaviour for varying sliding velocities and SiC dispersion of composites (a) Load vs Wear rate, (b) Load vs. SWR, (c) Load vs. CoF.

Table 9
ANOVA responses for W*R* and SWR.

	WR		SWR		COF	
Parameters	**F-value**	**p-value**	**F-value**	**p-value**	**F-value**	**p-value**
A-Load	89.39	< 0.0001	105.09	< 0.0001	50.66	< 0.0001
B-Sliding Velocity	11.05	0.004	13.25	0.002	2.63	0.1235
C-SiC Filler	64.53	< 0.0001	319.39	< 0.0001	139.15	< 0.0001
AB	1.22	0.2841	2.51	0.1318	0.0452	0.8342
AC	0.5464	0.4699	8.11	0.0111	4.72	0.0442
BC	6.13	0.0241	3.22	0.0905	107.91	< 0.0001
A^2	0.4341	0.5188	1.58	0.226	5.39	0.0329
B^2	15.57	0.001	4.85	0.0418	51.53	< 0.0001
C^2	157.48	< 0.0001	0.4929	0.4921	6.18	0.0236
R^2	0.9432		0.9642		0.9559	
Adjusted R^2	0.9132		0.9453		0.9325	
Predicted R^2	0.8654		0.9135		0.8971	

Table 10
Comparison of results of regression model and experimental trials.

Number	Load	Sliding Velocity	SiC Filler	Wear Rate (W*R*)	Specific Wear Rate (SWR)	Coefficient of Friction (CoF)
1	30	5.046	5.889	341.542	0.047	0.359
2	30	5.000	6.000	371.556	0.048	0.368
Error %				8.78	2.12	2.50

parameters on the wear performance of RCC (Figures Figs. 9–12). Variations in applied load and sliding velocity strongly govern all tribological responses, while the level of SiC reinforcement controls the stability, sensitivity, and predictability of the composite behaviour. At lower SiC content (2 wt%), the response surfaces for W*R* and SWR are smooth and gradual, indicating steady and predictable wear behaviour across the investigated range of loads and velocities. The close agreement between experimental data points and the predicted surfaces confirms the reliability of the regression model and reflects uniform stress distribution and stable fiber matrix interaction. Frictional force and COF at this level remain relatively low and consistent, signifying moderate frictional resistance and stable sliding behaviour. However, the limited filler content restricts the overall enhancement in wear resistance [25,29]. The composite reinforced with 4 wt% SiC exhibits the most balanced tribological response. Both W*R* and SWR surfaces show reduced wear values with controlled curvature, indicating improved resistance under moderate to severe operating conditions. Although slight deviations appear at higher loads and velocities, the majority of data points align well with the predicted surfaces, suggesting effective dispersion of SiC and strong interfacial bonding. The FF and COF surfaces at this composition display uniform gradients and tighter data clustering, reflecting enhanced load-bearing capacity, improved surface hardness, and stable frictional characteristics [43]. These features collectively indicate that 4 wt% SiC provides optimal reinforcement, ensuring consistent performance with minimal variability. At higher SiC content (6 wt%), the response surfaces become steeper and

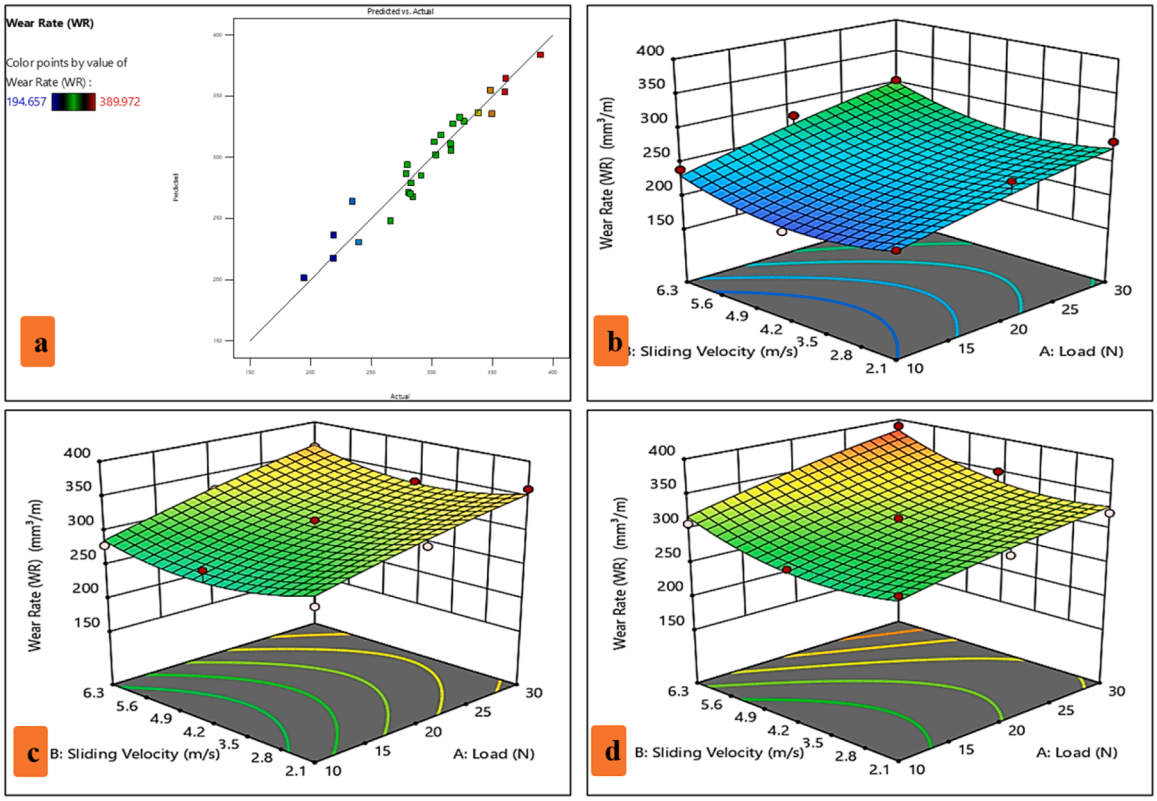


Fig. 9. 3D surface analysis of WR of RCC composites Load Vs Sliding velocity (a) predicted vs. actual, (b) 2 wt% SiC, (c) 4 wt% SiC, (d) 6 wt% SiC.

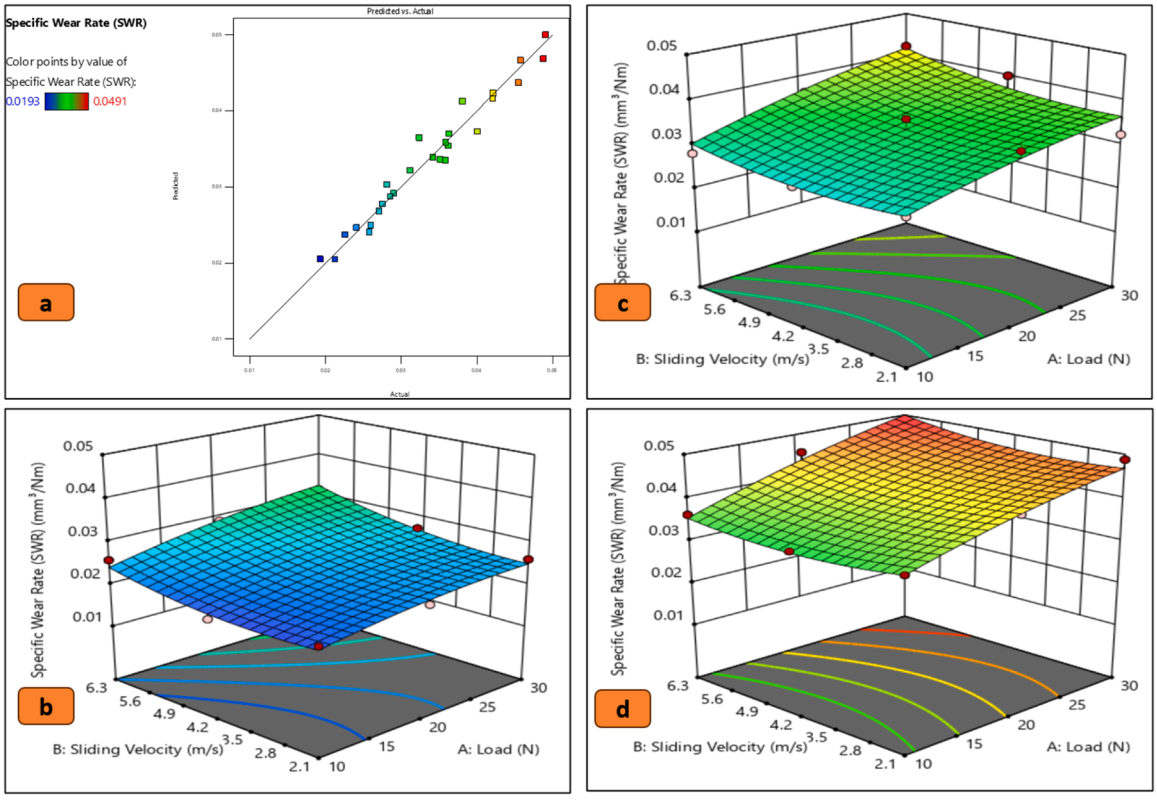


Fig. 10. 3D surface analysis of SWR of RCC composites Load Vs Sliding velocity (a) predicted vs. actual, (b) 2 wt% SiC, (c) 4 wt% SiC, (d) 6 wt% SiC.

more irregular, particularly at elevated loads and sliding velocities. While frictional force increases significantly due to enhanced interfacial interactions and mechanical interlocking, the WR, SWR, and COF responses show increased scatter and sensitivity to test parameters. This

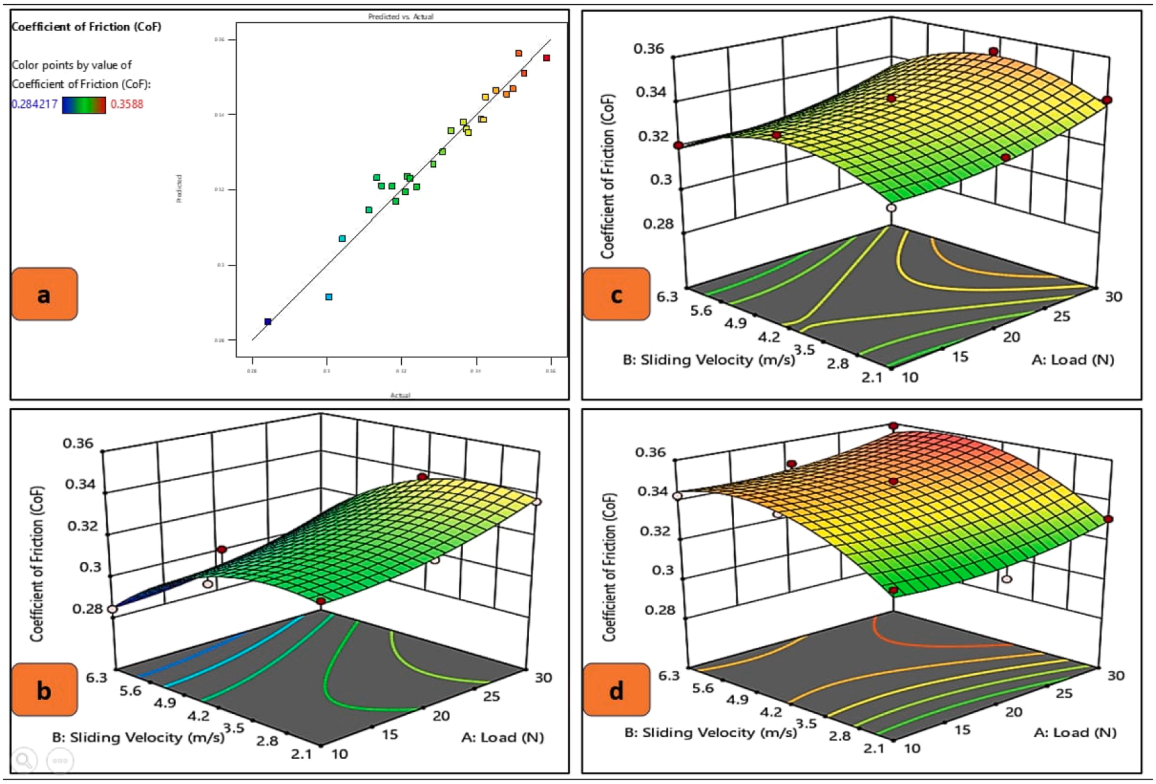


Fig. 11. 3D surface analysis of CoF of RCC composites Load Vs Sliding velocity (a) predicted vs. actual, (b) 2 wt% SiC, (c) 4 wt% SiC, (d) 6 wt% SiC.

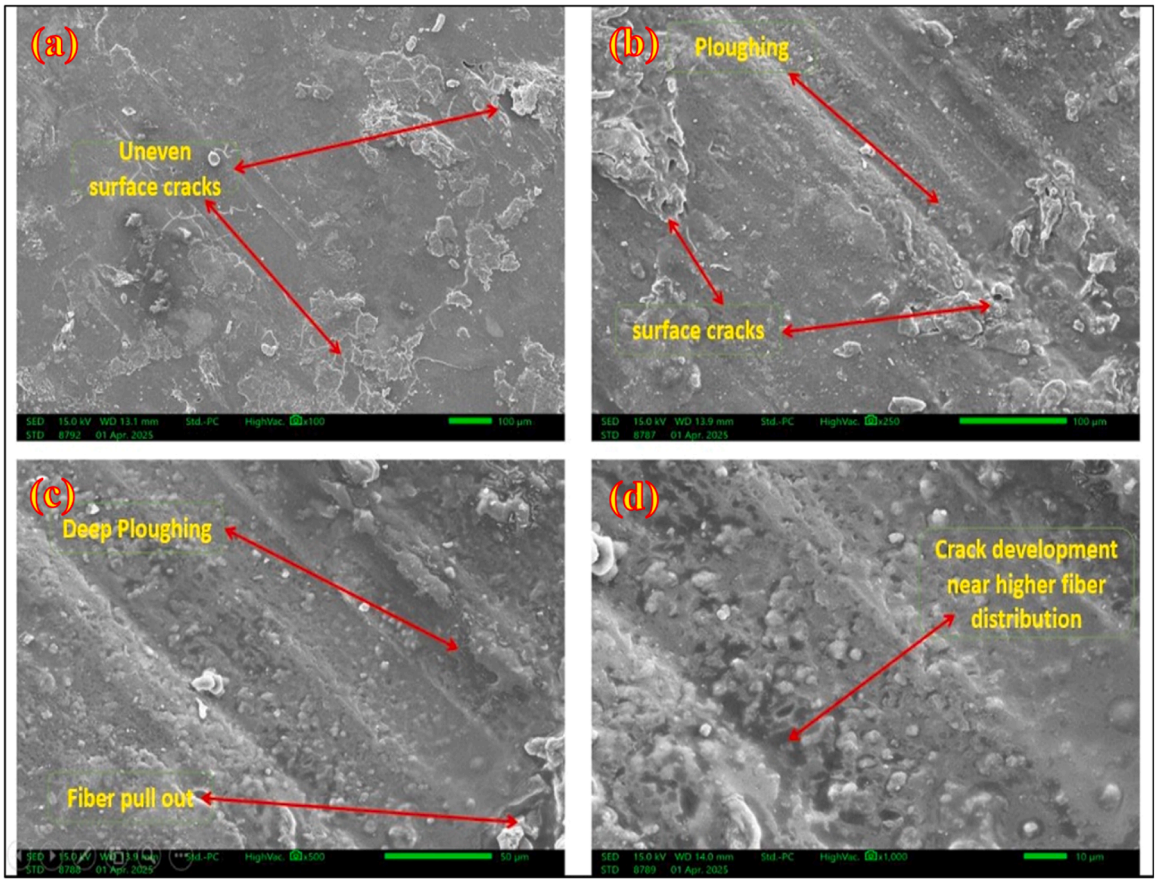


Fig. 12. SEM images of 2 wt% SiC dispersed RCC in different magnifications (a) 100x, (b) 250x, (c) 500x, (d) 1000x.

behaviour is attributed to partial agglomeration and non-uniform dispersion of SiC particles, which locally alters contact mechanics and reduces the predictability of the tribological response [23].

3.8. SEM results

SEM examination of worn surfaces provides that the influence of SiC content on the dominant wear mechanisms and interfacial integrity of RCC composites. For the 2 wt% SiC dispersed composite, the presence of uneven surfaces whereas the ploughing and deep ploughing layer along the wear track indicates material adhesion between the mating surfaces, which contributes to fiber pull-out due to direct abrasive wear (Fig. 12 a-d). However, matrix cracking caused by localized stress concentration is evident, along with progressive crack propagation driven by combined frictional and thermal stresses [10,23]. Despite these effects, the fibers and fillers remain relatively uniformly distributed, suggesting stable but limited reinforcement. The 4 wt% SiC composite exhibits a comparatively smoother worn surface with fewer pores and a more distinct fiber and matrix interfacial layer (Fig. 13 a-d). The formation of a continuous transfer layer and the CNSP fillers lubrication resulting in minimizing the surface damage and friction [21,45]. Although signs of fiber pull-out and crack initiation are present, their reduced frequency indicates improved load transfer and stronger interfacial bonding. These features confirm that 4 wt% SiC provides effective reinforcement and enhanced wear resistance under dry sliding conditions. The synergistic interaction between CNSP-derived carbonaceous transfer film and uniformly dispersed 4 wt% SiC particles promoted the formation of a stable tribo-layer, thereby reducing direct metal–composite contact and enhancing wear resistance. In contrast, the 6 wt% SiC composite shows pronounced matrix cracking, extensive fiber pull-out, and ploughing marks, indicating the dominance of abrasive wear mechanisms (Fig. 14 a-d). These characteristics suggest uneven filler dispersion and localized stress accumulation, resulting in partial reinforcement [25,46]. The tribo-layer formed in the other compositions was comparatively unstable due to either inadequate reinforcement or excessive SiC agglomeration, leading to repeated layer fracture and higher material loss.

Overall, from the morphological observations, it could be deduced that at 2 wt% SiC, the larger inter-particle spacing and lower reinforcement density provide insufficient hard-particle support to effectively bear and redistribute the applied contact stresses, allowing greater matrix deformation and abrasive/ploughing wear. Increasing the SiC content to 4 wt% reduces the inter-particle spacing and establishes a more effective load-bearing network, while the hard SiC particles restrict plastic deformation, improve interfacial load transfer, and stabilize the carbon-rich tribo-layer derived from CNSP, thereby reducing direct asperity contact and material removal. However, at 6 wt% SiC, the reduced particle spacing promotes particle–particle interaction and agglomeration, generating local stress concentrations and weakly bonded regions; these regions act as crack initiation sites and facilitate tribo-layer fragmentation and particle pull-out, ultimately increasing wear.

4. Conclusion

Hybrid polymer composites using Ricinus communis aro-waste fiber hybridized with Cashew nutshell and SiC fillers were fabricated and subjected to thermal and tribological properties evaluation. The following were the major conclusions obtained:

- The microstructural analysis of the hybrid composites showed the distribution of fibers and fillers with the matrix, thus reducing the pores and voids while, the EDX spectra analysis confirms the NaOH treatment, presence of SiC and bio fillers with their respective peaks. the XRD analysis shows that, as the SiC content increases in the RCC composites, the peaks generally show decreasing intensity for 2 wt%,

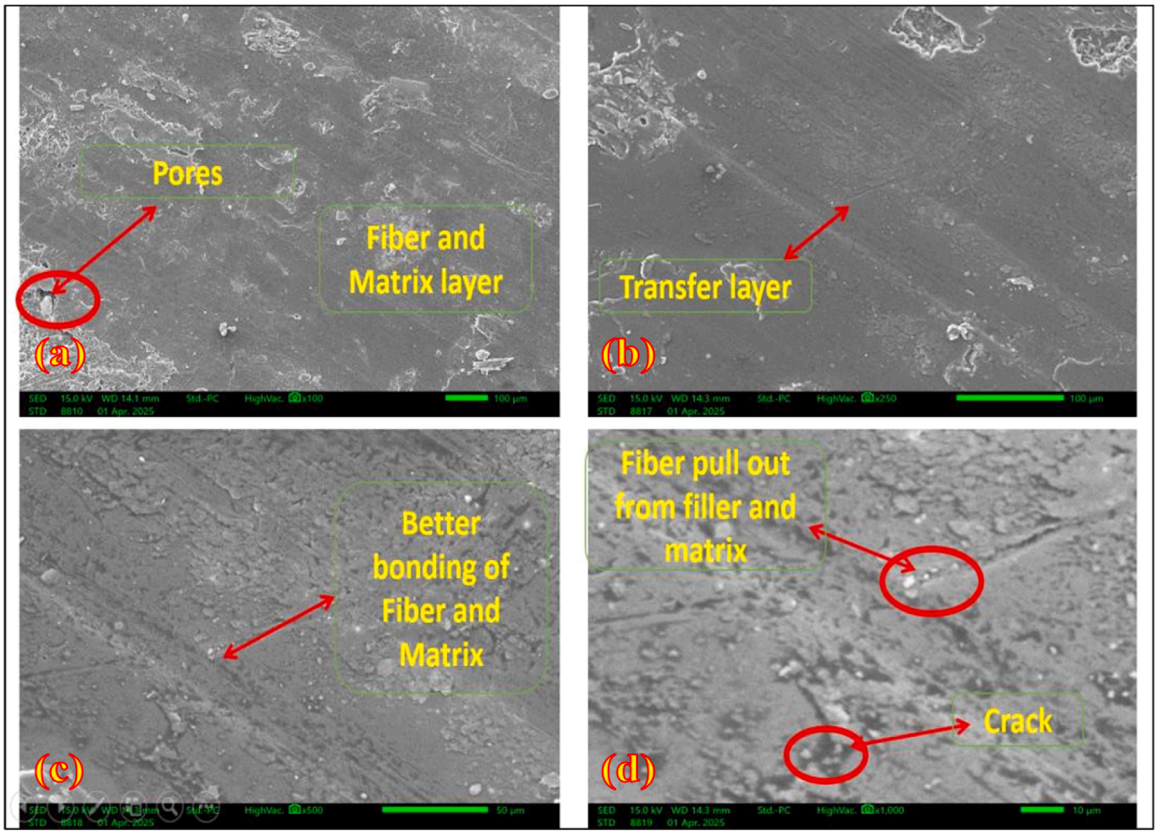


Fig. 13. SEM images of 4 wt% SiC dispersed RCC in different magnifications (a) 100x, (b) 250x, (c) 500x, (d) 1000x.

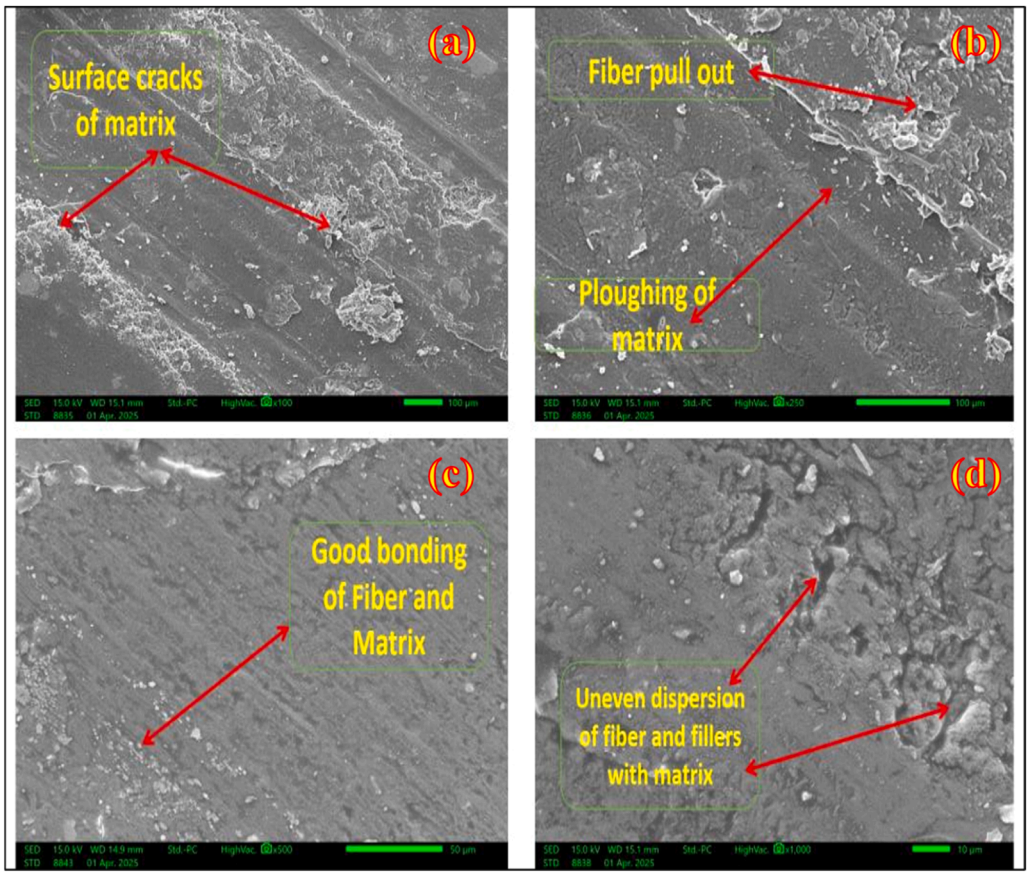


Fig. 14. SEM images of 6 wt% SiC dispersed RCC in different magnifications (a) 100x, (b) 250x, (c) 500x, (d) 1000x.

4 wt% and 6 wt% RCC samples indicating the phase change from crystallinity to amorphous condition.

- The thermal analysis showed that the optimal thermal performance is observed at 2 wt% and 4 wt% SiC, of onset and end temperatures ranging at 355 °C to 450 °C balancing improved resistance towards degradation and acceptable residue, while higher filler content may lead to degradation irregularities and structural compromises.
- The density of the RCC is in the range of 1.58–1.64 g/cm^3 making them highly suitable for lightweight applications. Increase in water absorption is found for higher SiC dispersed RCC due to the presence of increased pores and voids making the composite swell and weaker. The hardness of the material also increased linearly and consistent with increment in SiC content due to the filler particles distribution.
- The wear analysis of the SiC dispersed RCC showed that increase in wear parameters with respect to higher load of 30 N and sliding velocities at 6.3 m/s, while the optimal filler loadings (2 wt% to 4 wt %) can result in better wear behaviour of the composites in all conditions. Also, the presence of CNSP filler providing the self-lubricating layers under higher load and pressure surfaces resulting in reduced wear of the composites.
- The integrated 3D response analysis confirms that increasing SiC content improves frictional resistance and load-bearing capability, but excessive filler addition leads to variability in wear behaviour. Among the investigated compositions, the RCC composite with 4 wt % SiC demonstrates the most favourable combination of low wear, stable frictional response, and high model predictability at an 80 mm wear track diameter, making it the most suitable composition for dry sliding tribological conditions, which was also observed in the SEM analysis.
- Overall, observations confirm that 4 wt% SiC dispersed RC fiber composites offer the most favourable balance between interfacial bonding, wear resistance, and surface stability representing a suitable material for the structural and frictional component applications.

CRediT authorship contribution statement

R. Gopinath: Writing – review & editing, Validation. **G. Manikandan:** Writing – original draft, Validation, Data curation. **G. Rajeshkumar:** Resources, Investigation, Formal analysis. **L. Rajeshkumar:** Writing – review & editing, Validation, Methodology, Formal analysis. **P. Senthil Kumar:** Writing – original draft, Methodology, Investigation, Formal analysis. **T.P. Sathishkumar:** Formal analysis, Data curation, Conceptualization.

Declaration of Competing Interest

The authors declare that they have no known competing financial interests or personal relationships that could have appeared to influence the work reported in this paper.

Acknowledgement

Authors sincerely acknowledge the characterization support provided by Alliance University – Sophisticated Testing and Instrumentation Centre (AU-STIC), Alliance University, Bangalore, India.

Appendix A. Supporting information

Supplementary data associated with this article can be found in the online version at doi:10.1016/j.nxmate.2026.103418.

Data Availability

No new data is generated during this research work. All data generated or analyzed during this study are included in this published article

References

[1] D. Wong, G. Fabito, S. Debnath, M. Anwar, I.J. Davies, A critical review: recent developments of natural fiber/rubber reinforced polymer composites, Clean. Mater. 13 (2024) 100261.

[2] I. Elfaleh, F. Abbassi, M. Habibi, F. Ahmad, M. Guedri, M. Nasri, C. Garnier, A comprehensive review of natural fibers and their composites: an eco-friendly alternative to conventional materials, Results Eng. 19 (2023) 101271.

[3] J.J. Andrew, H.N. Dhakal, Sustainable biobased composites for advanced applications: recent trends and future opportunities–a critical review, Compos. Part. C Open. Access. 7 (2022) 100220.

[4] M. Li, Y. Pu, V.M. Thomas, C.G. Yoo, S. Ozcan, Y. Deng, A.J. Ragauskas, Recent advancements of plant-based natural fiber–reinforced composites and their applications, Compos. Part B Eng. 200 (2020) 108254.

[5] D. Jaiswal, G.L. Devnani, G. Rajeshkumar, M.R. Sanjay, S. Siengchin, Review on extraction, characterization, surface treatment and thermal degradation analysis of new cellulosic fibers as sustainable reinforcement in polymer composites, Curr. Res. Green. Sustain. Chem. 5 (2022) 100271.

[6] N.F. Ismail, N.A. Mohd Radzuan, A.B. Sulong, N. Muhamad, C.H. Che Haron, The effect of alkali treatment on physical, mechanical and thermal properties of Kenaf Fiber and polymer epoxy composites, Polymers 13 (12) (2021) 2005, https://doi.org/10.3390/polym13122005.

[7] R. Venkatesh, Processing and fabrication of hemp natural fiber-blended polypropylene composite: characteristics study, J. Inst. Eng. (India) Ser. D. (2024) 1–5.

[8] Saha, S., Das, S., & Rahman, M.Z. (2025). Hybridization in natural fiber composites: enhanced performance and sustainability. Composites Part B: Engineering, 112986.

[9] P. Senthil Kumar, T.P. Sathishkumar, L. Rajeshkumar, Characterization of novel cellulosic fiber extracted from agro-waste of Ricinus communis plant for sustainable green composite materials, Biomass Convers. Biorefin. 15 (7) (2025) 11199–11215.

[10] N. Chand, M. Fahim, Tribology of natural fiber polymer composites, Woodhead publishing, 2020, https://doi.org/10.1016/C2018-0-04814-8.

[11] R.A. Ibrahim, Tribological performance of polyester composites reinforced with agricultural wastes, Tribol. Int. 90 (2015) 463–466.

[12] T.P. Mohan, K. Kanny, Tribological properties of nanoclay-infused banana fiber reinforced epoxy composites', J. Tribol. 141 (2019) 052003.

[13] A.A.A. Talib, A. Jumahat, M. Jawaid, N. Sapiai, A.L. Leao, Effect of wear conditions, parameters and sliding motions on tribological characteristics of basalt and glass fibre reinforced epoxy composites, Materials 14 (3) (2021) 701.

[14] F.M. Khan, A.H. Shah, S. Wang, S. Mehmood, J. Wang, W. Liu, X. Xu, A comprehensive review on epoxy biocomposites based on natural fibers and bio-fillers: challenges, recent developments and applications, Adv. Fiber Mater. 4 (4) (2022) 683–704.

[15] G.O. Joseph, S. Adali, G. Bright, B. Sithole, Nanofiller/natural fiber filled polymer hybrid composite: a review, J. Eng. Sci. Technol. Rev. 14 (5) (2021).

[16] P. Kumar, M. Kumar, Natural nano-fillers materials for the bio-composites: a review, J. Indian. Chem. Soc. 99 (10) (2022) 100715.

[17] Y. Handa, T. Kato, Effects of Cu powder, BaSO4 and cashew dust on the wear and friction characteristics of automotive brake pads', Tribol. Trans. 39 (2) (1996) 346–353.

[18] I. Ilker Sugozu, I. Mutlu, A. Keskin, Friction and wear behaviour of ulexite and cashew in automotive brake pads, Mater. Tehnol. 49 (5) (2015) 751–758.

[19] P.A.P. Mamza, I.A. Okele, P.O. Nkeonye, Studies on the rheological properties of cashew nut shell powder, no. anacardium accidentale and carbon black on natural rubber vulcanisates, Compos. Mater. Int. J. CMAIJ 1 (1) (2016) 009–018, 2016.

[20] T.P. Sathishkumar, S.A. Kumar, P. Navaneethakrishnan, I. Siva, N. Rajini, 'Influence of cashew nut shell filler on tribological behaviors of natural-fiber-reinforced epoxy composite', Sci. Eng. Compos. Mater. 25 (4) (2018) 761–772.

[21] S. Rajendran, G. Palani, A. Veerasimman, U. Marimuthu, K. Kannan, V. Shanmugam, Biochar from cashew nut shells: a sustainable reinforcement for enhanced mechanical performance in hemp fibre composites, Clean. Eng. Technol. 20 (2024) 100745.

[22] T.P. Sathishkumar, R. Nagarajan, S.O. Ismail, V.V. Pruthiviraaj, A.B. Prabakaran, A. Saravanakumar, M.S. Ali, Characterization of banana and sisal fiber fabrics reinforced epoxy hybrid biocomposites with cashew nut shell filler for structural applications, BioResources 19 (4) (2024) 775.

[23] M.M. Samy, V. Raghunathan, D.L. Singaravelu, Investigation on the tribological behavior of aluminium titanate ceramic-based non-asbestos brake pads for passenger cars, J. Aust. Ceram. Soc. 62 (2025) 1213–1225.

[24] R. P Venkatesh, Silicon carbide embedded polyester composite enriched by kevlar fiber via compression mould: performance study, J. Inst. Eng. (India) Ser. D. (2024) 1–6.

[25] Y. Thooyavan, L.A. Kumaraswamidhas, R.E. Raj, J.S. Binoj, Influence of SiC micro and nano particles on tribological, water absorption and mechanical properties of basalt bidirectional mat/vinyl ester composites, Compos. Sci. Technol. 219 (2022) 109210.

[26] A. Behera, J. Dehury, B.P. Rayaguru, The consequence of SiC filler content on the mechanical, thermal, and structural properties of a jute/kevlar reinforced epoxy hybrid composite, Silicon 15 (15) (2023) 6509–6519.

[27] P. Satishkumar, K.S.R. Kumar, R. Chebolu, J. Giri, T. Sathish, A. Fatehmulla, Impact of different parameters in tribological properties of enset ventricosum/terminalia arjuna fibers/SiO2 filler incorporation, J. Mater. Res. Technol. 33 (2024) 3826–3836.

[28] P. Dhiravidamani, D. Jagadeesh, S. Al Obaid, R. Venkatesh, Influence of sisal-glass fiber/SiC combinations on behaviour of hybrid epoxy composite synthesized by advanced hot compression technique, J. Polym. Res. 31 (6) (2024) 181.

[29] X. Ma, Z. Li, M. Li, C. Lei, D. Xia, Q. Yang, J. Wu, Effect of silicon carbide content on thermal, mechanical, and tribological properties of resin-based friction materials, Polym. Compos. 46 (13) (2025) 12571–12586.

[30] M.N. Pervez, F. Shafiq, Z. Sarwar, M.M. Jilani, Y. Cai, Multi-response optimization of resin finishing by using a taguchi-based grey relational analysis, Materials 11 (3) (2018) 426.

[31] I. Iliyasu, J.B. Bello, M.N. Dibal, A.N. Oyedeji, K.A. Salami, E.O. Oyedeji, Response surface methodology for the optimization of the effect of fibre parameters on the physical and mechanical properties of deleb palm fibre reinforced epoxy composites, Sci. Afr. 16 (2022) e01269.

[32] K. Saada, S. Amroune, A. Belaadi, M. Zaoui, I.M. Alshaikh, D. Ghernaout, Enhancing the mechanical characteristics of eco-friendly composite materials: Taguchi and RSM optimization, J. Nat. Fibers 21 (1) (2024) 2427704.

[33] M.J. Paternina Reyes, J. Unfried Silgado, J.F. Santa Marín, H.A. Colorado Lopera, L.A. Espitia Sanjuán, Cashew nutshells: a promising filler for 3D printing filaments, Polymers 15 (22) (2023) 4347.

[34] T.P. Sathishkumar, L. Rajeshkumar, N. Rajini, S. Sivalingam, R. Gopinath, S. Santhoshkumar, M. Ramesh, Effects of cashew nutshell biofillers on the mechanical and thermal behaviour of Basalt/Hibiscus vitifolius hybrid fabrics reinforced polymer biocomposites, Sci. Rep. 14 (1) (2024) 27636.

[35] R. Venkatesh, Synthesis of CNT fiber with different stacking-made polyester composite via compression mold: mechanical behavior study, J. Inst. Eng. (India) Ser. D. (2024) 1–5.

[36] B.D. Agarwal, L.J. Broutman, K. Chandrashekhara, Analysis and performance of fiber composites, John Wiley & Sons, 2017.

[37] S. Biswas, A. Satapathy, A. Patnaik, Effect of ceramic fillers on mechanical properties of bamboo fiber reinforced epoxy composites: a comparative study, Adv. Mater. Res. 123–125 (2010) 1031–1034.

[38] H. Alamri, I.M. Low, Effect of water absorption on the mechanical properties of nanoclay filled recycled cellulose fibre reinforced epoxy hybrid nanocomposites', Compos. Part A Appl. Sci. Manufact. 44 (2013) 23–31.

[39] M.W. Dewan, M.K. Hossain, M. Hosur, S. Jeelani, Thermomechanical properties of alkali-treated jute–polyester/nanoclay biocomposites fabricated by VARTM process, J. Appl. Polym. Sci. 128 (2013) 4110–4123.

[40] M.I. Ibrahim, N.M. Bakhori, A.M. Nor, R. Mohammad, S.A.A. Aziz, M.M. Daud, M. Z. Hassan, Central composite design for optimization of kenaf-reinforced epoxy composite bonding performance, Bioresources 19 (1) (2024) 605.

[41] I. Iliyasu, J.B. Bello, M.N. Dibal, A.N. Oyedeji, K.A. Salami, E.O. Oyedeji, Response surface methodology for the optimization of the effect of fibre parameters on the physical and mechanical properties of deleb palm fibre reinforced epoxy composites, Sci. Afr. 16 (2022) e01269.

[42] B. Murali, B.M. Vijaya Ramnath, D. Rajamani, E.A. Nasr, A. Astarita, H. Mohamed, Experimental investigations on dry sliding wear behavior of Kevlar and natural fiber-reinforced hybrid composites through an RSM–GRA hybrid approach, Materials 15 (3) (2022) 749.

[43] S. Thirupathi, A. Solai, S.V. Pitchumani, V. Gopalan, E. Mallichetty, Evaluation of surface response of SiC and fly ash-filled Prosopis juliflora fibre-reinforced epoxy composites under dry sliding wear conditions using Taguchi method', J. Eng. Appl. Sci. 71 (1) (2024) 157.

[44] Bawono, B. Haniel, P.W. Anggoro, Optimization of characteristics polymer composite reinforced kenaf and jute fiber using taguchi-response surface methodology approach, J. Nat. Fibers 20 (2) (2023) 2204453.

[45] V. Raghunathan, S. G, V. Ayyappan, R. Srisuk, D. Lenin Singaravelu, S. M. Rangappa, S. Siengchin, Synergetic effects of zeolite and molybdenum disulfide on the tribological performance of hybrid fiber-based brake pads, Proc. Inst. Mech. Eng. Part. J J. Eng. Tribology (2025) 13506501251385054.

[46] R. Venkatesh, Surface-treated jute fiber-blended epoxy composite featured with SiC via injection molding process: characteristics study, J. Inst. Eng. (India) Ser. D. (2024) 1–5.